

Breaking the Pre-Planning Barrier: Real-Time Adaptive Coordination of Mission and Charging UAVs Using Graph Reinforcement Learning

Yuhan Hu^{1*}, Yirong Sun^{3*}, Yanjun Chen^{2,3}, Xinghao Chen^{2,3}

¹School of Cyber Science and Technology, Sun Yat-sen University, Shenzhen, China

²Department of Computing, The Hong Kong Polytechnic University, Hong Kong, China

³Digital Twin Institute, Eastern Institute of Technology, Ningbo, China

huyuhan6666@126.com

Abstract

Unmanned Aerial Vehicles (UAVs) are pivotal in applications such as search and rescue and environmental monitoring, excelling in intelligent perception tasks. However, their limited battery capacity hinders long-duration and long-distance missions. Charging UAVs (CUAVs) offers a potential solution by recharging mission UAVs (MUAVs), but existing methods rely on impractical pre-planned routes, failing to enable organic cooperation and limiting mission efficiency. We introduce a novel multi-agent deep reinforcement learning model named **Heterogeneous Graph Attention Multi-agent Deep Deterministic Policy Gradient (HGAM)**, designed to dynamically coordinate MUAVs and CUAVs. This approach maximizes data collection, geographical fairness, and energy efficiency by allowing UAVs to adapt their routes in real-time to current task demands and environmental conditions without pre-planning. Our model uses heterogeneous graph attention networks (GATs) to present heterogeneous agents and facilitate efficient information exchange. It operates within an actor-critic framework. Simulation results show that our model significantly improves cooperation among heterogeneous UAVs, outperforming existing methods in several metrics, including data collection rate and charging efficiency.

Introduction

UAVs are increasingly used in diverse applications such as search and rescue, environmental monitoring, and mobile crowd sensing (MCS). A critical challenge in these missions, particularly in dynamic and complex environments, is effective path planning. UAVs must navigate within a specified sensing range, avoid obstacles, and efficiently reach points of interest (PoIs) for data collection. However, their limited battery capacity often restricts operational efficiency, leading to mission interruptions or delays, which is especially problematic for emergency or long-duration missions. To mitigate battery limitations, prior research has explored UAV recharging at fixed or mobile bases (Mou et al. 2020) (Liu, Piao, and Tang 2020) (Liu et al. 2023). However, these methods require UAVs to fly additional distances for charging, increasing time and energy consumption and extending mission duration, thereby reducing overall efficiency. The concept of "aerial refueling" was introduced by (Zhu et al. 2022), where CUAVs serve as mobile charging stations, providing wireless charging to MUAVs during

*These authors contributed equally.

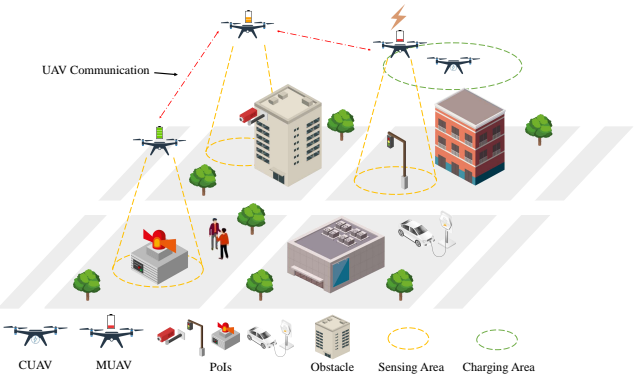


Figure 1: MUAVs and CUAVs adaptive coordination.

flight. This approach reduces mission completion time and enhances flexibility but still relies on pre-set flight routes, limiting adaptability in real-world scenarios. We propose a shift from pre-set routes to dynamic cooperation, where CUAVs autonomously provide charging support to extend MUAV operational time. This method offers greater flexibility to adapt to changing mission requirements and environmental conditions. However, traditional path planning methods often fail to meet the demands of complex, multi-objective UAV deployments. We address these challenges by considering a more realistic mission environment for CUAV-MUAV cooperation. **Specifically**, we focus on: **(a)** eliminating pre-set routes, allowing CUAVs and MUAVs to learn dynamic cooperation; **(b)** operating with only local field-of-view information without shared observations between UAVs; and **(c)** enabling continuous spatial actions rather than discrete movements. Our contributions are threefold:

- We introduce a novel multi-agent deep reinforcement learning model, **Heterogeneous Graph Attention Multi-agent Deep Deterministic Policy Gradient (HGAM)**, for dynamically coordinating MUAVs and CUAVs. It enables real-time route adjustments, allowing UAVs to respond to evolving mission requirements without pre-planned routes, thus maintaining operational continuity.
- HGAM models the dynamic state as a heterogeneous graph, aggregates agent information using GATs, and utilizes an actor-critic framework for continuous action

learning. The model's training and convergence are enhanced through N-step returns and prioritized experience replay techniques.

- Comparative simulations demonstrate that our model significantly improves cooperation among heterogeneous UAVs, outperforming existing methods in metrics such as data collection rate and charging efficiency and so on.

Related Work

Charging Issues in UAV Path Planning

To address energy constraints, several studies have introduced fixed-ground charging stations, allowing UAVs to recharge and resume their missions. However, this approach reduces task efficiency due to the additional flight paths required for recharging. For instance, the option deep Q-network (option-DQN) algorithm (Mou et al. 2020) was proposed within a discrete action Deep Reinforcement Learning (DRL) framework, enabling efficient UAV path planning while ensuring timely charging at fixed stations. (Liu et al. 2019) combined the Ape-X framework with the actor-critic method, using convolutional neural networks and prioritized experience replay to enhance data collection efficiency and charging. However, these methods implicitly assume fixed charging stations, requiring UAVs to travel extra distances, increasing time and energy consumption.

Mobile Charging Solutions

Advancements in wireless charging have led to mobile charging stations for UAVs, addressing real-time power needs. (Liu et al. 2023) employed ground charging vehicles as mobile power sources with pre-set routes, using DQN to train policies for UAVs to choose between sensors and charging vehicles. (Xu et al. 2022) deployed two UAVs to cooperatively collect data, where the primary UAV wirelessly charged from an auxiliary UAV with a larger battery capacity. To manage complex cooperative tasks, they combined the multi-agent policy gradient (MADDPG) (Lowe et al. 2020) algorithm with the option framework (Bacon, Harb, and Precup 2017), achieving multi-agent hierarchical policies for data collection, charging, and task termination. (Dou, Zhang, and Sun 2024) treated UAVs and mobile charging stations as two types of agents, designing mixed discrete-continuous actions. UAVs needed to decide on tasks or charging and determine stay durations based on a pre-determined PoIs visit order, while mobile charging stations selected charging locations and durations. (Zhu et al. 2022) introduced “aerial charging,” allowing CUAVs to wirelessly recharge MUAVs in flight, reducing mission time and increasing flexibility, though this approach is limited by the need for pre-set routes.

Path Planning with Graph and DRL Methods

Graph neural networks (GNNs) have been employed to manage the complex relationships in graph-structured data, making them suitable for tasks involving mobile users and UAVs. (Dai et al. 2022) combined relational graph convolutional networks with Monte Carlo tree search, achieving superior performance in UAV data collection tasks. The

GAT (Veličković et al. 2017) further improves node feature aggregation by using a self-attention mechanism.

Several studies have integrated GAT with DQN. (Dai et al. 2020) applied graph convolutional reinforcement learning (DGN) (Jiang et al. 2018) to optimize signal coverage for multiple UAVs. (Ye et al. 2022) used gated recurrent units (GRUs) (Cho et al. 2014) to store long-term information, enhancing robustness with a random policy based on the soft Bellman function (Haarnoja et al. 2017).

Novelties of HGAM

Existing models often restrict UAV action space to discrete levels within a DQN framework. In contrast, a hierarchical GAT model (Ryu, Shin, and Park 2020) within an actor-critic framework facilitates both low-level and high-level policy training, enhancing cooperation and competition among agents. Building on this, (Li, Luo, and Xie 2021) has refined the critic and actor networks to train heterogeneous agents for various objectives.

Our work advances this research by focusing on UAV cooperation in more complex scenarios than (Zhang et al. 2022) and (Chen et al. 2022). Routes are not predefined, and UAVs do not share a common field of view. The HGAM model enables UAVs to perform continuous spatial actions and facilitates synchronous cooperation between MUAVs and CUAVs. This is the first exploration of simultaneous cooperation between MUAVs and CUAVs with continuous actions, without pre-set routes or shared fields of view.

Background

Partially Observable Markov Decision Process

A Partially Observable Markov Decision Process (POMDP) (Ghosh et al. 2021) extends a Markov Decision Process (MDP) and is defined by the tuple $(S, A, T, R, \Omega, O, \gamma)$. At time t , an agent i receives a partial observation $o_t^i \in O$ from the global state $s_t \in S$ and selects an action $a_t^i \in A$ based on policy π_i , with $a_t^i \sim \pi_i(\cdot | o_t^i; \theta)$. The environment transitions from s_t to s_{t+1} via the transition function $T(s_{t+1} | s_t, a_t)$, where a_t represents actions taken by all agents. Each agent receives a reward $r_t^i \in R$, and the observation function $\Omega(o_{t+1} | s_{t+1}, a_t)$ provides the probability of obtaining o_{t+1} from s_{t+1} .

The goal in a POMDP is to maximize the expected discounted reward $\mathbb{E} [\sum_{t=0}^{\infty} \gamma^t r_t]$, where the discount factor γ balances the importance of immediate and future rewards.

Multi-agent Deep Deterministic Policy Gradient

DRL algorithms are categorized into value-based (Watkins and Dayan 1992) and policy-based (Sutton et al. 1999) methods. Value-based approaches, such as Q-Learning and DQN, optimize the state-action value function $Q(s, a) = \mathbb{E}[R]$ to derive action preferences, while policy-based methods, like Reinforce, directly optimize the policy $J(\theta^{\mu}) = \mathbb{E}[R]$. The actor-critic (Konda and Tsitsiklis 1999) framework combines these methods, with the actor learning a policy that maps states to actions, and the critic estimating the value function to guide the actor's updates.

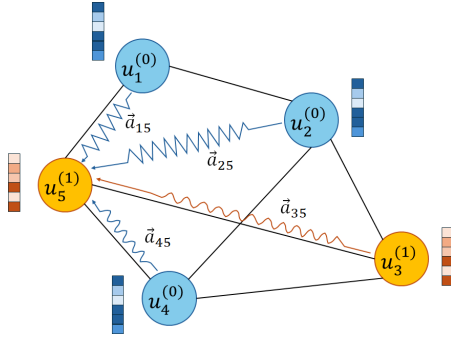


Figure 2: Heterogeneous graph attention network.

Deep Deterministic Policy Gradient (DDPG) (Lillicrap et al. 2019) extends the actor-critic framework to continuous action spaces, using deep neural networks for both the actor and critic. The actor outputs deterministic actions, while the critic estimates the value function. DDPG stabilizes training with target networks and adds noise via Ornstein-Uhlenbeck process (Uhlenbeck and Ornstein 1930).

MADDPG extends DDPG to multi-agent environments. Each agent has an independent actor network $\mu_i(o_i; \theta_i)$ that learns a policy based on local observations, and a critic network $Q(\mathbf{o}, \mathbf{a}; \theta_i)$ that evaluates the value function based on all agents' observations and actions. The critic updates using Temporal Difference (TD) error, minimizing the loss function $\mathcal{L}(\theta_i)$ to improve policy learning.

Graph Attention Network

GAT is a deep learning model for processing graph-structured data. It captures node relationships and allocates attention weights dynamically during learning. For a node i , GAT aggregates information from neighboring nodes $\mathcal{N}(i)$ using a self-attention mechanism, expressed as $h_i^l = \sigma \left(\sum_{j \in \mathcal{N}(i)} \alpha_{ij}^l W^l h_j^l \right)$, where α_{ij}^l is the attention coefficient determined by $\alpha_{ij}^l = \text{softmax}_j(e_{ij}^l)$ and $e_{ij}^l = \text{LeakyReLU}(a^l \cdot [W^l h_i^l || W^l h_j^l])$. This allows each node to adjust its focus based on the relevance of neighboring nodes, modeling complex graph relationships.

Problem Formulation

System Model

The task environment comprises a fixed three-dimension area with stationary obstacles $\mathcal{B} \triangleq \{1, 2, \dots, B\}$ and randomly distributed PoIs $\mathcal{P} \triangleq \{1, 2, \dots, P\}$. Two types of UAVs are used: MUAVs $\mathcal{M} \triangleq \{1, 2, \dots, M\}$ for data collection and CUAVs $\mathcal{C} \triangleq \{1, 2, \dots, C\}$ for recharging MUAVs. Both are collectively represented as $\mathcal{U} \triangleq \{1, 2, \dots, U\}$.

MUAVs have a specific sensing range and collect data from PoIs within this range. CUAVs have a charging range for wirelessly recharging MUAVs. UAVs move horizontally at different altitudes to avoid collisions with each other but can still collide with obstacles, walls, or other UAVs at the same altitude. All UAVs have a communication range that

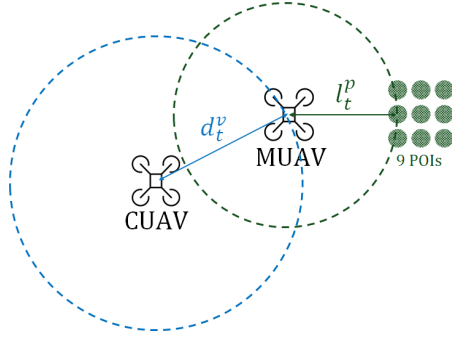


Figure 3: Illustration of CUAV and MUAV task. d_t^v and l_t^p stand for charging radius and sensing radius, respectively.

covers the entire environment, allowing continuous information exchange. Each MUAV starts with maximum energy Er_0^m , insufficient to complete the task alone. The energy consumption at each time step is: $Ed_t^m = \beta \times c_t^m + \kappa \times l_t^m$ where c_t^m is the data collected, l_t^m is the distance traveled, and β and κ are energy conversion coefficients. CUAVs provide a constant energy e_0 per time step. If a MUAV's energy is fully recharged, additional charging is ineffective. CUAVs can only charge one MUAV at a time, prioritizing the closest one when multiple MUAVs are within range. Table 1 presents the main symbols and their descriptions used in the task environment of this paper.

Table 1: Main Symbol Descriptions

Symbol	Description
\mathcal{B}	Set of obstacles
\mathcal{P}	Set of PoIs
\mathcal{U}	Set of all UAVs
\mathcal{M}	Set of MUAVs
\mathcal{C}	Set of CUAVs
c_t^m, l_t^m	Data collected and distance moved by MUAV at time t
m_t^p	Remaining data volume at time t
Er_t^m, Ec_t^m, Ed_t^m	MUAV energy: remaining, charged, consumed at time t
d_t^u, l_t^u	Direction and distance to the object u
$\mathcal{L}(u)$	Set of objects in the field of view
$G = (V, E)$	Graph (nodes, edges)
$\mathcal{N}(u)$	Set of neighbors in the graph
n_u	Priority Experience Replay (PER) tree of the UAV
π_u, Q_u	Policy and Q-function of the UAV

Evaluation Metric

The primary objective for MUAVs is to complete data collection tasks efficiently and fairly. For CUAVs, the goal is to assist MUAVs in timely recharging, preventing task failures due to MUAV power depletion. To evaluate these objectives, this paper considers three metrics for the performance of the MUAV policy π and two metrics for the performance of the CUAV policy π .

Data Collection Ratio. Let m_0^p represent the initial data volume for each PoI. The total amount of data collected

by all MUAVs up to episode T is denoted by $D(\pi) = \sum_{t=1}^T \sum_{m=1}^M c_t^m$. The data collection ratio is defined as:

$$C_T(\pi) = \frac{D(\pi)}{\sum_{p=1}^P m_p^p} \quad (1)$$

Geographical Fairness. To ensure data diversity and uniformity within the workspace, $\omega_T(\pi)$ adopts the Jain's fairness index (Jain et al. 1984). $\frac{m_T^p}{m_0^p}$ represents the remaining data volume of each up to episode T . Higher values of $\omega_T(\pi)$ indicate a more uniform data collection across all PoIs.

$$\omega_T(\pi) = \frac{\left(\sum_{p=1}^P \frac{m_p^p}{m_0^p}\right)^2}{P \sum_{p=1}^P \left(\frac{m_p^p}{m_0^p}\right)^2} \quad (2)$$

Energy Usage Efficiency. Let Ed_T^m represent the energy consumed by a MUAV in flying and collecting data, Er_0^m represent the initial energy of the MUAV, and Ec_T^m represent the accumulated recharged energy of the MUAV. The energy usage efficiency of MUAVs is defined as:

$$v_T(\pi) = \frac{1}{M} \sum_{m=1}^M \frac{Ed_T^m}{Er_0^m + Ec_T^m} \quad (3)$$

Charging Efficiency. Let T represent the total number of steps in a single episode, and T_c represent the number of steps or times CUAV_c recharges MUAVs in an episode. Charging efficiency is measured by the total number of recharges as follows:

$$D_T(\pi) = \frac{1}{C} \sum_{c=1}^C \frac{T_c}{T} \quad (4)$$

Charging Fairness. Similar to geographical fairness, charging fairness is measured using Jain's fairness index. E_{\max} represents the maximum chargeable energy that an MUAV can receive, and $\frac{Ec_T^m}{E_{\max}}$ represents the accumulated recharged energy of an MUAV up to episode T . Charging fairness is defined as:

$$F_T(\pi) = \frac{\left(\sum_{m=1}^M \frac{Ec_T^m}{E_{\max}}\right)^2}{M \sum_{m=1}^M \left(\frac{Ec_T^m}{E_{\max}}\right)^2} \quad (5)$$

Problem Definition

For the data collection task, the UAV should find the optimal policy π^* to maximize multiple objectives. For MUAVs, π^* needs to maximize the objective $C_T(\pi) \cdot \omega_T(\pi)$; for CUAVs, π^* needs to maximize the objective $D_T(\pi) \cdot F_T(\pi)$. Meanwhile, MUAVs need to complete the task before the battery is depleted, and all UAVs must avoid collisions. The task objective formula is:

$$\pi^* = \arg \max_{\pi} (C_T(\pi) \cdot \omega_T(\pi), D_T(\pi) \cdot F_T(\pi)) \quad (6)$$

subject to $\forall m \in M, Ed_T^m < Er_0^m + Ec_m^T$.

State Space. Includes the 2D positions of all obstacles, 2D positions of PoIs, current remaining data volume, UAV 2D positions, remaining battery, charged battery, status, and attributes. Among them, the MUAV status includes $\{-1 : \text{battery depleted}; 0 : \text{flying}; 1 : \text{charging}\}$, and the CUAV status includes $\{0 : \text{flying}; 1 : \text{charging}\}$. The attribute of MUAV is 0, and the attribute of CUAV is 1.

Action Space. The actions of MUAV and CUAV are 2D angular velocities, i.e., $a_t^u = (x_t^u, y_t^u)$, where $x_t^u \in [-1, 1]$, $y_t^u \in [-1, 1]$. The a_t^u is normalized to ensure that each UAV moves the same distance at time slot t .

State Transition Function. $T(s_{t+1} \mid s_t, \mathbf{a}_t)$ represents the state transition probability function from time slot t to time slot $t+1$. It describes the probability that, after all UAVs execute the action \mathbf{a}_t in state s_t , the environment transitions to state s_{t+1} . The entire episode ends when a UAV collides or the MUAV's battery is depleted.

Observation Space. Due to the limited field of view of the UAVs, the MUAV can only observe part of the surrounding states. Due to the heterogeneity of the two types of UAVs, their observation values are different. The observation value of the MUAV is $o_t^m = \{\mathbf{l}_t, \mathbf{b}_t^u, \mathbf{p}_t^m, v_t^u, g_t^u, t, s_t^u, n^u\}$, while the observation value of the CUAV is $o_t^c = \{\mathbf{l}_t, \mathbf{b}_t^u, \mathbf{e}_t^c, v_t^u, g_t^u, t, s_t^u, n^u\}$.

Where $\mathbf{l}_t = \{l_t^1, l_t^2, \dots, l_t^n\}$ represents n horizontal laser beams emitted by the UAV, with each laser length representing the distance from the UAV to a nearby obstacle. If an obstacle is detected, l_t^n represents the distance to the obstacle; otherwise, it represents the total length of the laser beam.

$\mathbf{b}_t^u = \{d_t^v, l_t^v\}, \forall v \in \mathcal{L}(u)$, where $\mathcal{L}(u)$ represents all UAVs within the field of view of UAV_u, d_t^v represents the 2D direction to UAV_v, and l_t^v represents the distance to UAV_v.

$\mathbf{p}_t^m = \{d_t^p, l_t^p, m_t^p\}, \forall p \in \mathcal{L}(p)$, where $\mathcal{L}(p)$ represents all PoIs within the field of view of UAV_m, d_t^p represents the 2D direction to PoI_p, l_t^p represents the distance to PoI_p, and m_t^p represents the remaining data volume of PoI_p.

$\mathbf{e}_t^c = \{Er_t^m, Ec_t^m\}, \forall m \in \mathcal{M}$, represents the remaining battery and charged battery of all MUAVs, where $Er_t^m \in [0, 1]$, $Ec_t^m \in [0, 1]$.

v_t^u represents the 2D angular velocity of current UAV_u. $g_t^u = \{0, 1\}$ indicates whether UAV_u is in a stationary rotation state, as detailed below. t represents the current time slot. s_t^u represents the state of UAV_u. $n^u = \{0, 1\}$ indicates the attribute of UAV_u.

Observation Function. $\Omega(o_{t+1} \mid s_{t+1}, \mathbf{a}_t)$ represents the probability of obtaining the partial observation value o_{t+1} after all actions \mathbf{a}_t are executed, given the state s_{t+1} .

Reward Function. Due to the different policy goals, the reward functions for MUAVs and CUAVs also need to be set separately. The reward function for MUAVs is:

$$r_t^m = h_t^m + \iota_t^m - pl_t^m - pb_t^u \quad (7)$$

Where $h_t^m = w_c \times c_t^m$, is proportional to the data volume collected by the current MUAV_m; ι_t^m rewards the MUAV for collecting more PoIs. When the number of PoIs covered at time slot t is greater than that at time slot $t-1$, or the that is

closer to the MUAV, it gets a reward value $\iota_t^m = w_i$; pl_t^m is a penalty for MUAV if it rotates without collecting data; pb_t^u is a common penalty for UAVs if they collide with obstacles or walls or if the laser length is less than the threshold.

The reward function for CUAV is:

$$r_t^c = h_t^c + \iota_t^c - pl_t^c - pb_t^u \quad (8)$$

Where $h_t^c = w_e \times f_t$, w_e is the reward for effective charging of CUAV at time slot t , f_t is the fairness factor, specifically given by:

$$f_t = w_f f_{ct} + (1 - w_f) f_{rt} \quad (9)$$

$$f_{ct} = \frac{\left(\sum_{i=1}^n \min \left(\frac{Ec_i^i}{E_{\max}}, 1 \right) \right)^2}{n \times \sum_{i=1}^n \min \left(\frac{Ec_i^i}{E_{\max}}, 1 \right)^2} \quad (10)$$

$$f_{rt} = \frac{\left(\sum_{i=0}^n Er_t^i \right)^2}{n \times \sum_{i=0}^n Er_t^i} \quad (11)$$

Where f_{ct} represents the fairness of the charged battery levels of all MUAVs, and f_{rt} represents the fairness of the remaining battery levels of all MUAVs. w_f is an adjustable parameter; ι_t^c is the penalty for CUAV when it is not charging or performing ineffective charging, specifically given by:

$$\iota_t^c = w_d l_t^i + w_e Er_t^i \quad (12)$$

Where i is the MUAV with the lowest remaining battery at time slot t , l_t^i is the direct distance from CUAV to i , and w_d and w_e are penalty parameters. ι_t^c encourages the CUAV to move towards the lower-battery MUAV and charge it. pl_t^c is the penalty when the MUAV reaches the lowest battery threshold, calculated as:

$$pl_t^c = \begin{cases} plow_t^c, & \text{CUAV is not charging} \\ \frac{6}{5} \times plow_t^c, & \exists M_i \in \mathcal{M}, Er_t^i \geq 1 \text{ or } Ec_t^i \geq 1 \\ \frac{plow_t^c}{3}, & \exists M_i \in \mathcal{M}, Er_t^i \geq Er_{avg}^i \\ \frac{plow_t^c}{4}, & \text{otherwise.} \end{cases} \quad (13)$$

Where Er_{avg}^i is the average remaining battery level of all MUAVs at time slot t . When the CUAV is not in charging, the penalty is $plow_t^c$; when the CUAV charges an MUAV whose battery level has reached the threshold, the maximum penalty is $\frac{6}{5} \times plow_t^c$; when the CUAV's charging target has a remaining battery level greater than the average remaining battery level, the penalty is $\frac{plow_t^c}{3}$; when the CUAV does not meet any of the above conditions, the penalty is $\frac{plow_t^c}{4}$. Separate reward functions for MUAVs and CUAVs to reflect their different objectives, including data collection, fairness, effective charging, and penalties for inefficiencies.

SOLUTION: HGAM

State Representation using Graph. Given the presence of two types of heterogeneous agents, MUAV and CUAV, with different observation values, reward functions, and strategic goals, we use a heterogeneous graph to represent the relationship between agents. As shown in Figure 2, let

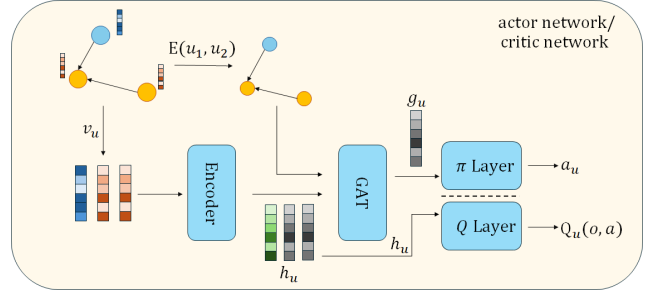


Figure 4: Illustration of our actor/critic network

$G = (V, E)$ represent a graph where V are the nodes (agents), and v_u is the feature vector of a node. Different colors in the vector indicate different attribute types of the agent. The edges $E = \{0, 1\}$ represent communication links between agents, where $E(u_1, u_2) = 1$ indicates that agents u_1 and u_2 can communicate and share information. Since UAVs are constantly moving, their communication relationships dynamically change, making graphs an appropriate representation of the current state.

Graph Feature Learning. Designing an effective network to learn useful information from heterogeneous graph input states is crucial. As illustrated in Figure 4, our network model consists of three main components: an encoder layer, a GAT layer, and an execution layer.

The encoder maps the features of all nodes v_u into embedding vectors h_u , formulated as: $h_u = f_u(v_u)$. The encoder is composed of a Multi-Layer Perceptron (MLP) that converts node features of different dimensions into embedding vectors of uniform dimensions.

The GAT layer aggregates information from neighboring nodes. For UAV u , the neighbor sets $\mathcal{N}(u) = \{N_{\text{local}}(u), N_{\text{global}}(u)\}$ that represent local and global neighbors, respectively, and the neighbor embedding vector sets $\mathcal{H}(u) = \{h_v \mid \forall v \in \mathcal{N}(u)\}$ are derived from the graph structure. The GAT layer employs attention mechanisms to manage relationships between UAVs and their neighbors:

$$g_u = t_u(h_u, \mathcal{H}(u)) = \sum_{v \in \mathcal{N}(u)} \alpha_{vu} \cdot Wh_v \quad (14)$$

where α_{vu} is the attention weight between UAV v and UAV u , representing the importance between them. It is calculated as:

$$\alpha_{vu} = \frac{\exp(\text{LeakyReLU}(a^\top [Wh_v || Wh_u]))}{\sum_{k \in \mathcal{N}(u)} \exp(\text{LeakyReLU}(a^\top [Wh_v || Wh_k]))} \quad (15)$$

The execution layer outputs Q values and action values through the Q layer and policy layer (π layer), respectively, both composed of MLPs. The Q layer of the critic network concatenates the embedding vectors h_u^Q and g_u^Q to compute the Q value for each UAV: $Q_u(\mathbf{o}, \mathbf{a}) = \psi_u(h_u^Q, g_u^Q)$. The policy layer of the actor network outputs actions a_u based on the embedding vectors h_u^π and g_u^π : $a_u = \mu_u(h_u^\pi, g_u^\pi)$.

Overall Framework

In the actor-critic framework, each agent has an independent actor network and critic network. The actor network selects actions based on the agent's observations, while the critic network evaluates the value of all agents' observations and actions to provide a current state score, guiding strategy updates. By training the model in this manner, MUAVs with only local graph information can select the globally optimal action. Our network model, based on the actor-critic framework, uses graphs of varying scales to model the current state. As shown in Figure 5, the actor network inputs the local graph of the current UAV, while the critic network inputs the global graph.

Actor Network and Local Graph. The actor network processes the relationship between the current UAV and its neighboring UAVs. The local graph of the current UAV includes three nodes: the UAV itself and the two nearest neighboring UAVs with each attribute, i.e., UAVs within the direct distance of the current UAV. Formally, let $\mathcal{N}_{\text{local}}(u) = \{v^{(0)}, v^{(1)} \mid \forall n \in \{(0), (1)\}, \forall w \in V_n, d(u, v) < d(u, w)\}$, where V_n represents the set of nodes that have the same attribute n . The node feature is the observed value of the UAV, $v_u = o_u$. By aggregating information from neighboring UAVs with different attributes, the current UAV can better learn strategies for cooperation, resulting in the embedded vectors h_u^π and g_u^π .

Critic Network and Global Graph. The critic network evaluates the current global environment. In the global graph, all nodes point to the current UAV, i.e., $\mathcal{N}_{\text{global}}(u) = \{v \mid \forall v \in V\}$. The features of all nodes in the global graph include both the observation and action values of the UAVs, i.e., $v_u = \text{concat}(o_u, a_u)$. By aggregating information from all UAVs, the critic network generates unique embedded vectors h_u^Q and g_u^Q for the current UAV, providing a comprehensive evaluation of the overall environment.

Actor-critic Network Update. This model is trained and executed under the Centralized Training Decentralized Execution (CTDE) paradigm. During centralized training, the critic network has access to global information and utilizes a global graph. During decentralized execution, each UAV carries a small processor that allows the actor network to run offline. By inputting the local graph of the current UAV, the UAV executes tasks based on the action values output by the actor network.

The critic network updates its parameters ϕ_u by minimizing the loss function $\mathcal{L}(\phi_u)$:

$$\mathcal{L}(\varphi_u) = \mathbb{E}_{(\mathbf{o}, \mathbf{a}, \mathbf{r}, \mathbf{o}') \sim D} \left[\left(r_u + \gamma \psi'_u (h_u^{Q'}, g_u^{Q'}; \varphi'_u) - \psi_u (h_u^Q, g_u^Q; \varphi_u) \right)^2 \right] \quad (16)$$

where ψ'_u is the Q-layer of the target critic network; $h_u^{Q'}$ and $g_u^{Q'}$ are obtained from the coding layer and the GAT layer of the target critic network, as follows: $h_u^{Q'} = f'_u(o'_u, a'_u; w'_h)$, $g_u^{Q'} = t'_u(\mathcal{H}(u'); w'_t)$, $a'_u = \mu'_u(h_u^{\pi'}, g_u^{\pi'}; \theta'_u)$

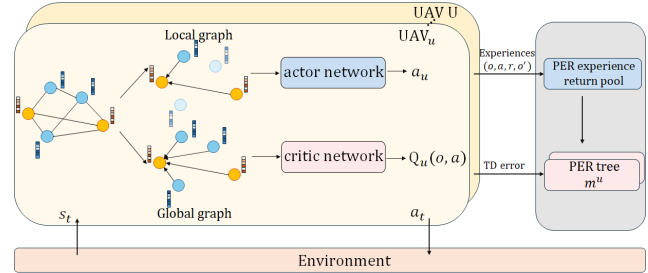


Figure 5: Overall framework of HGAM

The actor network updates its parameters θ_u based on the following gradient:

$$\nabla_{\theta_u} J(\theta_u) = \mathbb{E}_{(\mathbf{o}, \mathbf{a}) \sim D} [\nabla_{\theta_u} \mu_u (h_u^\pi, g_u^\pi; \theta_u) \nabla_{a_u} \psi_u (h_u^Q, g_u^Q) \mid a_u = \mu_u (h_u^\pi, g_u^\pi; \theta_u)] \quad (17)$$

It is important to note that the coding layers and GAT layers of both the critic and actor networks are used to calculate different embedded vectors and participate in parameter selection and update execution.

Training Methodology Design

Dilemma Detection Mechanisms

To encourage MUAVs to efficiently perform data collection tasks, we adopt the dilemma detection and reward mechanisms proposed in (Wei et al. 2022) to facilitate model training and convergence. The dilemma detection mechanism identifies whether a MUAV has fallen into a local optimal rotation during training, which can hinder overall task performance. Normally, when a MUAV is flying as expected, the overlapping area $o_{t, t+1}$ between its positions at consecutive time steps is maximized. However, if there exists a time step t' where $o_{t, t'} > o_{t, t+1}$, it indicates that the MUAV is in a local rotation, signaling a suboptimal strategy.

N-step Return and Prioritized Experience Replay

To improve the efficiency of model training, we employ training techniques such as PER(Schaul et al. 2015) and N-step return(Sutton and Barto 2018), as described in (Wei et al. 2022). The N-step return technique extends the reward horizon for the UAV, allowing it to consider cumulative rewards over N future steps, rather than only the immediate reward. The cumulative reward is calculated as follows: $\lambda_t^u = r_t^u + \gamma r_{t+1}^u + \dots + \gamma^{N-1} r_{t+N-1}^u$. The target Q-value is then updated as: $y_t^u = \lambda_t^u + \gamma^N \psi'_u (h_u^{Q'}, g_u^{Q'}; \varphi'_u)$. PER uses the TD error $\delta_m^u = y_t^u - \psi_u (h_u^Q, g_u^Q; \varphi_u)$ as the priority for experience replay, selecting experiences for training from the experience return pool. The weight of experience m is calculated as:

$$\zeta^u(m) = \frac{(\delta_m^u)^\alpha}{\sum_k (\delta_k^u)^\alpha}, \forall m \quad (18)$$

where α is a parameter that controls the degree of prioritization. Consequently, the loss function of the critic network is

updated as:

$$\begin{aligned} \mathcal{L}(\varphi_u) = & \mathbb{E}_{(o, a, r, o') \sim D} \left[\zeta^u(m) \times \left(\lambda_t^u + \gamma^N \psi'_u \left(h_{u, t}^{Q'}, g_{u, t}^{Q'}; \varphi'_u \right) \right. \right. \\ & \left. \left. - \psi_u \left(h_{u, t}^Q, g_{u, t}^Q; \varphi_u \right) \right)^2 \right] \end{aligned} \quad (19)$$

Overall Training Process

The overall training process is summarized in a Table in the Supplementary material. Before training begins, each UAV initializes its actor network π_u and critic network Q_u , with UAVs of the same attribute sharing a common critic network.

The target critic network Q'_u and target actor network π'_u are initialized by copying the parameters of their respective original networks. Each UAV is equipped with a PER tree m_u to store TD errors and initializes an empty experience return pool M . At the start of each episode, the environment is reset, and the UAVs obtain their initial observations o_t^u . Actions a_t^u are then performed according to policy π_u : $a_t^u = \pi_u(o_t^u) = \mu_u(h_{u, t}^\pi, g_{u, t}^\pi; \theta_u) + \mathcal{O}$, where \mathcal{O} represents Gaussian noise added for exploration during training. The UAVs interact with the environment, obtaining the next observation o_{t+1} and reward r_t , and store current experience in the experience return pool M . The UAVs update their PER trees using a fixed upper limit. After a certain number of episodes e_{min} , the model starts training while continuing to explore. The model selects a batch of experiences H from M based on the current time step t and its PER tree indices, calculates the weight of each experience $\zeta^u(H)$ using Eq. 18, and updates the actor and critic network gradients using Eq. 17 and Eq. 19, respectively. The target networks are updated according to the update frequency f_{soft} using the following formulas: $\varphi'_u = \tau \varphi_u + (1 - \tau) \varphi'_u$ and $\theta'_u = \tau \theta_u + (1 - \tau) \theta'_u$. The priority of experience H is updated accordingly. If an episode ends due to task completion, collision, or power depletion, the episode terminates, and a new episode begins. The total reward, number of time slots, and data collection rate convergence visualization during model training are shown in the supporting materials.

EXPERIMENT

Environment Setting. All experiments were conducted with a single NVIDIA RTX 4090 GPU. The task environment was a $16 \times 16 \times 3$ grid workspace where PoIs were randomly distributed to enhance model robustness. The number of MAUVs is 2 and CUAV is 1. We set 100 PoIs, with their data volumes randomly generated within $[0, 1]$. The system's sensing, charging, and field of view ranges were 1.0, 1.5, and 4 units, respectively. UAVs had a radius of 0.2 units, PoIs 0.1 units. Each UAV could move up to 0.13 units per time step and collect up to 0.2 units of data per hour per PoI. The environment also included specific laser settings, with a maximum energy capacity E_{max} of 1, and the horizontal laser count and length set to 12 and 4 units, respectively.

The system employed several penalties and rewards to guide learning. UAV collisions incurred a 100-point penalty,

and a penalty of 2 was applied if the laser length fell below the threshold. Stationary MAUVs and those not collecting data were penalized by 2 and 1 points, respectively. Rewards included a MAUV data collection reward of $w_c = 0.5$, a 0.02 reward for MAUV movement (w_l), and a 1.6 reward for effective CUAV charging (w_e). The fairness factor w_f was set to 0.5, with penalties for CUAVs not charging set at $w_d = -0.2$ and $w_e = -0.08$. MAUVs faced a 100-point penalty for low-threshold power $plow_c^t$, and the maximum episode time was limited to 700.

Hyperparameter Setting. The actor network's final layer used a Tanh activation function to limit outputs to $[-1, 1]$, while other layers employed LeakyReLU to prevent information loss, considering observation values also ranged from $[-1, 1]$. The critic network had a hidden layer dimension of 128, and the actor network's hidden layer dimension was 64. Learning rates for the critic and actor networks were 0.001 and 0.0001, respectively. The discount factor γ was set at 0.98, with a target network update parameter τ of 0.01 and an N-step return value of 3. The target network update frequency f_{soft} was configured to 50, and training commenced after a minimum of 50 episodes e_{min} . The experience replay buffer could store up to 100,000 experiences, with a batch size of 128. The priority sampling parameter α in $\zeta^u(m)$ was set to 0.6.

Visualization. Figure 6 illustrates the route visualization for two MUAVs and one CUAV. In Figure 6(a), only the routes of the MUAVs are shown. The two MUAVs demonstrate effective coordination, with no overlapping routes. Despite having access only to local view information, the routes of the MUAVs successfully cover most of the PoIs, including those in biased and less frequently visited areas, resulting in a high data collection rate. In Figure 6(b), the route of the CUAV is added. It is evident that the CUAV's route closely follows the paths of the two MUAVs, initially aligning with the purple MUAV's route and later resembling the red MUAV's route. This allows the CUAV to provide wireless charging to both MUAVs at different times without any overlap. Throughout the operation, all UAVs effectively avoid collisions with obstacles.

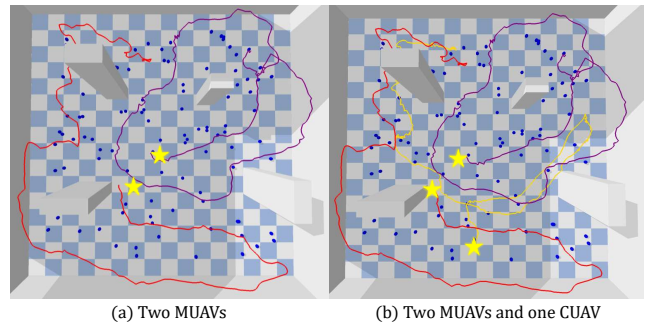


Figure 6: Evaluation visualization of two MUAVs and CUAV with local view

Comparing with three Baselines

Table 2: Performance - train and evaluate with **local** view

Metric	Greedy	MADDPG	MAAC	HGAM
C	0.333	0.630	0.185	0.928
ω	0.374	0.633	0.222	0.929
v	0.273	0.333	0.042	0.298
D	0.127	0.429	0.521	0.613
F	0.590	0.957	0.500	0.969

Table 3: Performance - train and evaluate with **global** view

Metric	Greedy	MADDPG	MAAC	HGAM
C	0.333	0.492	0.285	0.582
ω	0.374	0.540	0.136	0.610
v	0.273	0.305	0.023	0.422
D	0.127	0.403	0.000	0.370
F	0.590	0.905	1.000	0.989

Analysis. We evaluate the performance of our HGAM model against three baselines: Greedy, MADDPG, and MAAC (Iqbal and Sha 2019), considering task scenarios as training. We chose MADDPG and MAAC due to their focus on learning-for-consensus approaches, which are designed to operate effectively with local observations during execution. The comparison is conducted under two settings—local view and global view—with metrics categorized into MUAV-related (Data Collection Ratio C , Geographical Fairness ω , and Energy Usage Efficiency v) and CUAV-related (Charging Efficiency D and Charging Fairness F).

Local View Training and Evaluation. As presented in Table 2, HGAM excels in Data Collection Ratio (C) with a score of 0.928, far surpassing MADDPG (0.630), MAAC (0.185), and Greedy (0.333). It also leads in Geographical Fairness (ω) with 0.929, indicating effective and balanced data collection across PoIs, outperforming MADDPG (0.633), MAAC (0.222), and Greedy (0.374). While HGAM’s Energy Usage Efficiency (v) is slightly lower at 0.298 compared to MADDPG (0.333), it still outperforms MAAC (0.042) and is close to Greedy (0.273), showing a good balance between energy consumption and task performance. In Charging Efficiency (D), HGAM leads with 0.613, outperforming MADDPG (0.429), MAAC (0.521), and Greedy (0.127). HGAM also tops Charging Fairness (F) with 0.969, showing its ability to distribute charging resources equitably among MUAVs, surpassing MADDPG (0.957), MAAC (0.500), and Greedy (0.590).

Global View Training and Evaluation. To test our model’s robustness, we tried to train and evaluate those models with a global view under the same task setting, presented in Table 3. HGAM continues to lead in the Data Collection Ratio (C) with 0.582, though the gap with MADDPG (0.492) narrows. In Geographical Fairness (ω), HGAM scores 0.610, again outperforming MADDPG (0.540) and MAAC (0.136). For Energy Usage Efficiency (v), HGAM improves to 0.422, outperforming MADDPG (0.305) and

MAAC (0.023), demonstrating effective energy management with full visibility. In Charging Efficiency (D), HGAM scores 0.370, slightly lower than in the local view but still ahead of MAAC (0.000) and Greedy (0.127). In Charging Fairness (F), HGAM scores 0.989, nearly matching MAAC’s 1.000 and outperforming MADDPG (0.905) and Greedy (0.590).

Result. HGAM consistently outperforms the baselines across both MUAV and CUAV metrics in local and global view settings. It excels in data collection, fairness, and efficiency, demonstrating robustness in complex multi-agent environments. While there is a slight trade-off in energy usage efficiency compared to MADDPG, HGAM’s superior performance, especially in local view settings, underscores its effectiveness in UAV coordination tasks, establishing it as a robust solution for multi-agent UAV operations.

CONCLUSION

We propose the HGAM model, a novel multi-agent deep reinforcement learning model, that effectively coordinates MUAVs and CUAVs in real-time, without relying on pre-planned routes. By leveraging heterogeneous graph attention networks within an actor-critic framework, our model enhances cooperation among UAVs, leading to significant improvements in data collection, geographical fairness, and energy efficiency. Simulation results demonstrate that HGAM outperforms existing methods, proving its effectiveness in optimizing UAV missions for complex and dynamic environments.

References

Bacon, P.-L.; Harb, J.; and Precup, D. 2017. The option-critic architecture. In *Proceedings of the AAAI conference on artificial intelligence*, volume 31.

Chen, Y.; Song, G.; Ye, Z.; and Jiang, X. 2022. Scalable and transferable reinforcement learning for multi-agent mixed cooperative–competitive environments based on hierarchical graph attention. *Entropy*, 24(4): 563.

Cho, K.; Van Merriënboer, B.; Gulcehre, C.; Bahdanau, D.; Bougares, F.; Schwenk, H.; and Bengio, Y. 2014. Learning phrase representations using RNN encoder–decoder for statistical machine translation. *arXiv preprint arXiv:1406.1078*.

Dai, A.; Li, R.; Zhao, Z.; and Zhang, H. 2020. Graph convolutional multi-agent reinforcement learning for UAV coverage control. In *2020 International Conference on Wireless Communications and Signal Processing (WCSP)*, 1106–1111. IEEE.

Dai, Z.; Liu, C. H.; Ye, Y.; Han, R.; Yuan, Y.; Wang, G.; and Tang, J. 2022. AoI-minimal UAV crowdsensing by model-based graph convolutional reinforcement learning. In *IEEE INFOCOM 2022-IEEE conference on computer communications*, 1029–1038. IEEE.

Dou, J.; Zhang, H.; and Sun, G. 2024. Scheduling Drone and Mobile Charger via Hybrid-Action Deep Reinforcement Learning. *arXiv preprint arXiv:2403.10761*.

Ghosh, D.; Rahme, J.; Kumar, A.; Zhang, A.; Adams, R. P.; and Levine, S. 2021. Why generalization in rl is difficult: Epistemic pomdps and implicit partial observability. *Advances in neural information processing systems*, 34: 25502–25515.

Haarnoja, T.; Tang, H.; Abbeel, P.; and Levine, S. 2017. Reinforcement learning with deep energy-based policies. In *International conference on machine learning*, 1352–1361. PMLR.

Iqbal, S.; and Sha, F. 2019. Actor-attention-critic for multi-agent reinforcement learning. In *International conference on machine learning*, 2961–2970. PMLR.

Jain, R. K.; Chiu, D.-M. W.; Hawe, W. R.; et al. 1984. A quantitative measure of fairness and discrimination. *Eastern Research Laboratory, Digital Equipment Corporation, Hudson, MA*, 21: 1.

Jiang, J.; Dun, C.; Huang, T.; and Lu, Z. 2018. Graph convolutional reinforcement learning. *arXiv preprint arXiv:1810.09202*.

Konda, V.; and Tsitsiklis, J. 1999. Actor-critic algorithms. *Advances in neural information processing systems*, 12.

Li, Y.; Luo, X.; and Xie, S. 2021. Learning heterogeneous strategies via graph-based multi-agent reinforcement learning. In *2021 IEEE 33rd International Conference on Tools with Artificial Intelligence (ICTAI)*, 709–713. IEEE.

Lillicrap, T. P.; Hunt, J. J.; Pritzel, A.; Heess, N.; Erez, T.; Tassa, Y.; Silver, D.; and Wierstra, D. 2019. Continuous control with deep reinforcement learning. *arXiv:1509.02971*.

Liu, C. H.; Dai, Z.; Zhao, Y.; Crowcroft, J.; Wu, D.; and Leung, K. K. 2019. Distributed and energy-efficient mobile crowdsensing with charging stations by deep reinforcement learning. *IEEE Transactions on Mobile Computing*, 20(1): 130–146.

Liu, C. H.; Piao, C.; and Tang, J. 2020. Energy-efficient UAV crowdsensing with multiple charging stations by deep learning. In *IEEE INFOCOM 2020-IEEE conference on computer communications*, 199–208. IEEE.

Liu, N.; Zhang, J.; Luo, C.; Cao, J.; Hong, Y.; Chen, Z.; and Chen, T. 2023. Dynamic Charging Strategy Optimization for UAV-Assisted Wireless Rechargeable Sensor Networks Based On Deep Q-network. *IEEE Internet of Things Journal*.

Lowe, R.; Wu, Y.; Tamar, A.; Harb, J.; Abbeel, P.; and Mordatch, I. 2020. Multi-Agent Actor-Critic for Mixed Cooperative-Competitive Environments. *arXiv:1706.02275*.

Mou, Z.; Zhang, Y.; Fan, D.; Liu, J.; and Gao, F. 2020. Research on the UAV-aided data collection and trajectory design based on the deep reinforcement learning. *Chinese Journal on Internet of Things*, 4(3): 42–51.

Ryu, H.; Shin, H.; and Park, J. 2020. Multi-agent actor-critic with hierarchical graph attention network. In *Proceedings of the AAAI Conference on Artificial Intelligence*, volume 34, 7236–7243.

Schaul, T.; Quan, J.; Antonoglou, I.; and Silver, D. 2015. Prioritized experience replay. *arXiv preprint arXiv:1511.05952*.

Sutton, R. S.; and Barto, A. G. 2018. *Reinforcement learning: An introduction*. MIT press.

Sutton, R. S.; McAllester, D.; Singh, S.; and Mansour, Y. 1999. Policy gradient methods for reinforcement learning with function approximation. *Advances in neural information processing systems*, 12.

Uhlenbeck, G. E.; and Ornstein, L. S. 1930. On the theory of the Brownian motion. *Physical review*, 36(5): 823.

Veličković, P.; Cucurull, G.; Casanova, A.; Romero, A.; Lio, P.; and Bengio, Y. 2017. Graph attention networks. *arXiv preprint arXiv:1710.10903*.

Watkins, C. J.; and Dayan, P. 1992. Q-learning. *Machine learning*, 8: 279–292.

Wei, K.; Huang, K.; Wu, Y.; Li, Z.; He, H.; Zhang, J.; Chen, J.; and Guo, S. 2022. High-performance UAV crowdsensing: A deep reinforcement learning approach. *IEEE Internet of Things Journal*, 9(19): 18487–18499.

Xu, J.; Kang, X.; Zhang, R.; Liang, Y.-C.; and Sun, S. 2022. Optimization for master-UAV-powered auxiliary-aerial-IRS-assisted IoT networks: An option-based multi-agent hierarchical deep reinforcement learning approach. *IEEE Internet of Things Journal*, 9(22): 22887–22902.

Ye, Z.; Wang, K.; Chen, Y.; Jiang, X.; and Song, G. 2022. Multi-UAV navigation for partially observable communication coverage by graph reinforcement learning. *IEEE transactions on mobile computing*, 22(7): 4056–4069.

Zhang, X.; Zhao, H.; Wei, J.; Yan, C.; Xiong, J.; and Liu, X. 2022. Cooperative trajectory design of multiple UAV base stations with heterogeneous graph neural networks. *IEEE Transactions on Wireless Communications*, 22(3): 1495–1509.

Zhu, K.; Yang, J.; Zhang, Y.; Nie, J.; Lim, W. Y. B.; Zhang, H.; and Xiong, Z. 2022. Aerial refueling: Scheduling wireless energy charging for UAV enabled data collection. *IEEE Transactions on Green Communications and Networking*, 6(3): 1494–1510.